Automatic Extraction of Cartographic Information from Airborne Interferometric SAR Data

Reinhold Huber[a] and Anselm Schmieder[b]

[a] Department of Computer Sciene, University of Salzburg, Austria

[b]Aero–Sensing Radarsysteme GmbH, c/o DLR Oberpfaffenhofen, Germany

ABSTRACT

Automatic classification of regions towards cartographic feature extraction by the airborne AeS–1 instrument is presented. We extract regions corresponding to cartographic features for the classes built–up area, forest, water and open area. Water and built–up area are extracted from the intensity image. The use of a DEM as additional source of information allows to distinguish built–up land and forest from all other classes. The mathematical tools for feature extraction from intensity and DEM data are fractal dimension estimation and mathematical morphology. The classification is done employing a decision tree.

Keywords: decision tree classifier, mathematical morphology, fractals, local statistics

1. INTRODUCTION

Extraction of cartographic information is a time–consuming process in the case of visual interpretation. High–accurate remotely sensed data as provided by the Aero–Sensing AeS–1 interferometric airborne SAR system operating in X–band make it possible to a least semi–automate the process of region extraction relevant to a cartographic map product. The purpose of the decision tree classification presented in this paper is not primarily to distinguish various land–use or land–cover classes, moreover the classified land–cover is an intermediate product further used to generate a bare–soil DEM by approximating height information in built–up and forest regions. Therefore, the final classes are built–up area, forest, water and open area, no distinction between different forest types etc. is attempted.

We will show how to use image processing and pattern recognition tools to automatically extract these information. The classification is performed by a sequential decision tree classifier. The thresholds for each decision layer are automatically derived from a training set using a simple threshold selection rule. Results of using parameters from local statistics of the SAR backscatter and fractal analysis of the DEM are presented and assessed.

The study area is a 5000 by 2048 pixel AES–1 scene containing the villages of Weßling, Oberpfaffenhofen and parts of Neugilching, Germany. The image is shown in figure 4(a). Backscatter and DEM data is used in the automatic processing towards cartographic feature extraction.

2. INTERFEROMETRIC SAR PRODUCTS

Interferometric processing of SAR data combines two single look complex (SLC) images. The images are coregistered at sub–pixel accuracy and an interferogram and a coherence map are derived. The generation of a Digital Elevation Model (DEM) requires further processing, i.e. flat–earth removal, phase noise reduction, phase unwrapping and phase–to–height conversion.[1]

Whereas in repeat–pass interferometry the most valuable information, e.g. for forest classification, is caused by the temporal decorrelation between the data takes from spaceborne platforms such as the ERS satellites,[2] this is not true for single–pass airborne operation such as the Aero–Sensing sensor AeS–1.[3] Temporal decorrelation takes no or limited place in single–pass interferometry, therefore this kind of interpretation is not applicable. On the other hand high accurate data is provided by the AeS-1 instrument; in our study data of spatial resultion of 1 by 1 meters and height accuracy of 0.5 meter for the DEM–product is used, which suggests an interpretation of the surface roughness.

Other author information: (Send correspondence to R.H.)
R.H.: Email: reini@cosy.sbg.ac.at; Telephone: +43-662-8044-6324 or +49-8153-281350; Fax: +49-8153-281543; Supported by the EC under a Leonardo Da Vinci Traineeship
A. S.: Email: anselm@jerry.as.op.dlr.de; Telephone: +49-8153-281350; Fax: +49-8153-281543
Aero–Sensing WWW: http://dv.op.dlr.de/aerosensing/

3. POST–PROCESSING OF INTERFEROMETRIC SAR DATA

We extract regions corresponding to cartographic features for the classes built–up area, forest, water and open area. Water and built–up area are extracted from the intensity image. The SAR backscatter characteristics for these two classes, mainly specular reflection over water and frequent corner reflection over built–up land offers a discrimination potential. The use of a DEM as additional source of information allows to distinguish built–up land and forest from all other classes. The mathematical tools for feature extraction from intensity and DEM data and for classification refinement are described below.

3.1. Fractal Dimension Estimation

To describe the roughness of the observed land surface we employ the idea of fractal dimension. Fractal dimension corresponds quite closely to the notion of roughness; the fractal dimension D of a flat surface is slightly larger than 2, the topological dimension of an ideally flat surface, and increases with increasing roughness towards 3. Fractals encountered in physical processes have the properties of statistical self–similarity and statistical invariance over a wide range of scales. Fractional Brownian motion (fBm), a generalization of Brownian motion, describes these properties.[4]

Migliaccio and Riccio[5] used the following formulation to analyze SAR data:

$$\Pr\Big(\frac{z(x+\Delta x, y+\Delta y) - z(x,y)}{\sqrt{\Delta x^2 + \Delta y^2}} < \delta\Big) = F(\delta), \tag{1}$$

where x denotes range and y azimuth direction, $F(\delta)$ is a cumulative distribution function.[6] The relationship between topological dimension and fractal dimension D is in this case given as

$$D = 3 - H, \tag{2}$$

where H is called the Hurst parameter.

The expectation of the height difference is given by

$$E[z(x+\Delta x, y+\Delta y) - z(x,y)] = \Sigma\sqrt{2/\pi}(\Delta x^2 + \Delta y^2)^{H/2}, \tag{3}$$

which is equal to

$$\log(E[|z(x+\Delta x, y+\Delta y) - z(x,y)|]) = H\log(\sqrt{\Delta x^2 + \Delta y^2}) + \log(\Sigma\sqrt{2/\pi}). \tag{4}$$

To estimate the Hurst parameter H and the value of Σ a linear regression is used with the logarithmically scaled observations of height and distance, e.g. a straight line is fitted to the linear model

$$\begin{aligned} z(d) &= Hd + a, \\ \text{where}\quad a &= \log(\Sigma\sqrt{2/\pi}), \\ \text{and}\quad d &= \log(\sqrt{\Delta x^2 + \Delta y^2}). \end{aligned} \tag{5}$$

From the slope of the regression line and formulas 4 and 2 we get an estimation of the locally observed fractal dimension.

3.2. Mathematical Morphology

Mathematical morphology is used to simplify image data preserving their essential shape characteristics and eliminating irrelevancies.[7] Mathematical morphology models images in an Euclidean N–space E^N, we restrict ourself to the consideration of the E^2 space, the space of binary images. Consider the sets A and B in the E^2 space, then the dilation $A \oplus B$ of A and B is defined by

$$A \oplus B = \{c \in E^2 | c = a + b \quad \text{for some} \quad a \in A \quad \text{and} \quad b \in B\}, \tag{6}$$

and the erosion $A \ominus B$ of A by B is defined by

$$A \ominus B\{x \in E^2 | x + b \in A \quad \text{for every} \quad b \in B\}. \tag{7}$$

Closing and opening are compound operations of dilation and erosion. The opening $A \circ S$ of image A by the structuring element S is defined by $A \circ S = A \ominus (A \oplus S)$. The closing $A \bullet S$ of image A by the structuring element S is defined as $A \bullet S = A \oplus (A \ominus S)$.

We will especially investigate the usage of iterated application of alternating sequences of openings and closings with structuring elements of growing size and alternating shape.

4. CARTOGRAPHIC PRODUCT GENERATION

The cartographic product is generated by classification of features from local statistics of the SAR intensity image and from fractal dimension estimation and classification from the DEM. Mathematical Morphology is employed throughout the process to achieve post-classification smoothing. The classification algorithm is depicted in figure 3 and described in detail below.

4.1. Local statistics features

The idea of local statistics is evaluation of statistical parameters of a small sliding window centered around the pixel under consideration and characterization of the central pixel by those parameters, e.g. the mean, variance, coefficient of variation if first order statistics turns out to be sufficient. Higher order statistics, i.e. co-occurrence matrix features,[8] is also frequently used to describe texture. The map shown in figure 4(b) is derived from the local standard deviation σ.

4.2. Fractal dimension estimation

The fractal dimension is also estimated in the neighborhood of the pixel in question by linear regression to the logarithmically scaled observations of the height values versus the distance to the central pixel. In figure 1(a) the linear regression of a window sampled from a forest region is shown, figure 1(b) shows the same for an area covered by grass. The slope of the regression line gives an estimation for the Hurst parameter. Figure 5(a) depicts the fractal

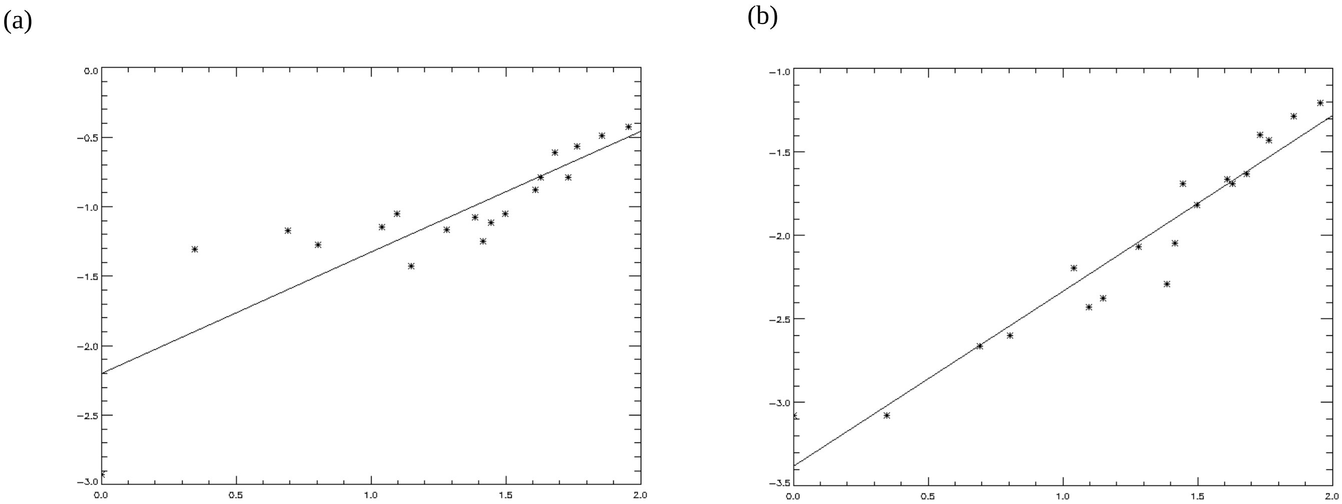

Figure 1. Fractal dimension estimation by linear regression for forest area (a) and open area (b). The horizontal axis is the logarithm of the distance to the central pixel d, the vertical axis is the logarithm of the height z, as given in equations (5).

dimension. In this image the fractal dimension of water is close to 2, the topological dimension of a surface, the fractal dimension of open area is remarkably higher than for forest.

4.3. Classification

The applied classification scheme is based on sequential binary decisions and combinations of the results. A similar decision tree algorithm was presented recently by Ferrazzoli et.al.[9] for multi-frequency polarimetric SAR data where decision thresholds were derived using a priori knowledge. To prevent repeated passes through the algorithm with different threshold settings a training set containing typical class prototypes are interactively selected prior for each classification step. Examining the class distributions of the considered features, e.g. the fractal dimension or the local σ, the following threshold selection rule turned out to be well suited and computationally more efficient, compared to a nearest neighbor classifier. Let m_1 and σ_1 be the mean and standard deviation of the considered feature for samples belonging to class 1, and m_2, σ_2 the values for class 1, respectively. The binary decision threshold t is given by

$$t = m_1 + (m_2 - m_1)\frac{\sigma_1}{\sigma_1 + \sigma_2} \quad \text{where} \quad m_2 > m_1. \tag{8}$$

4.4. Post-classification Smoothing by Mathematical Morphology

Mathematical morphology is used throughout the processing to eliminate misclassifications and to achieve homogeneous looking regions, which can be compared to the smoothing part of generalization in cartographic map production. Iterated morphological filter were introduced by Sternberg,[10] applied to single–look SAR images by Frery et.al.[11] and recently extended by Pei and Lai.[12] In our case the iterated morphological filter consists of a sequence of six repeated applications of closings and openings with structuring element of increasing size, i.e.

$$I_m = ((((((((((((I_c \circ S_1) \bullet S_1) \circ S_2) \bullet S_2) \circ S_3) \bullet S_3) \circ S_4) \bullet S_4) \circ S_5) \bullet S_5) \circ S_6) \bullet S_6) \tag{9}$$

where I_c is the classification result, I_m the morphologically improved image and the S_i the the structuring elements growing in size with index i. Figure 2 depicts the size and shape of the structuring elements S_i.

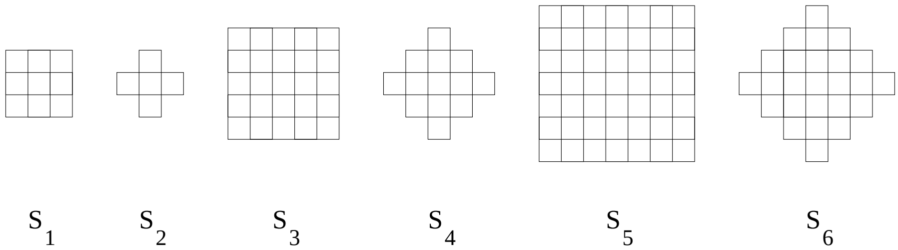

Figure 2. Size and shape of the sequence of structuring elements used for morphological filtering.

Figure 4(c) shows the result of iterated morphology applied to the classification from local statistics features. Figure 5(b) shows the closing of the classified fractal dimension.

4.5. Combination of Classification Results

Results are combined to extract the binary forest classification map I_f shown in figure 5(c) from the composite classification of forest and built-up area I_{fb}, see figure 5(b), and built-up area map I_b, see figure 4(c), by $I_f = I_{fb} \setminus I_b$.

Due to the used phase–unwrapping algorithms weakness over water areas, e.g. a low coherence area, the elevation contained in the DEM image I_d is corrected at all pixel positions (x, y) where the water is classified in map I_w. The water classification map I_w is also refined applying a minimum region thresholding, i.e. only connected regions containing at least a minimum number of pixels are accepted.

The maps I_b, I_f and I_w are finally fused together to end up with the combined classification map shown in figure 5(b), the remaining class I_o, in our case labeled as open area, are all pixels where $I_b \cup I_f \cup I_w = \emptyset$.

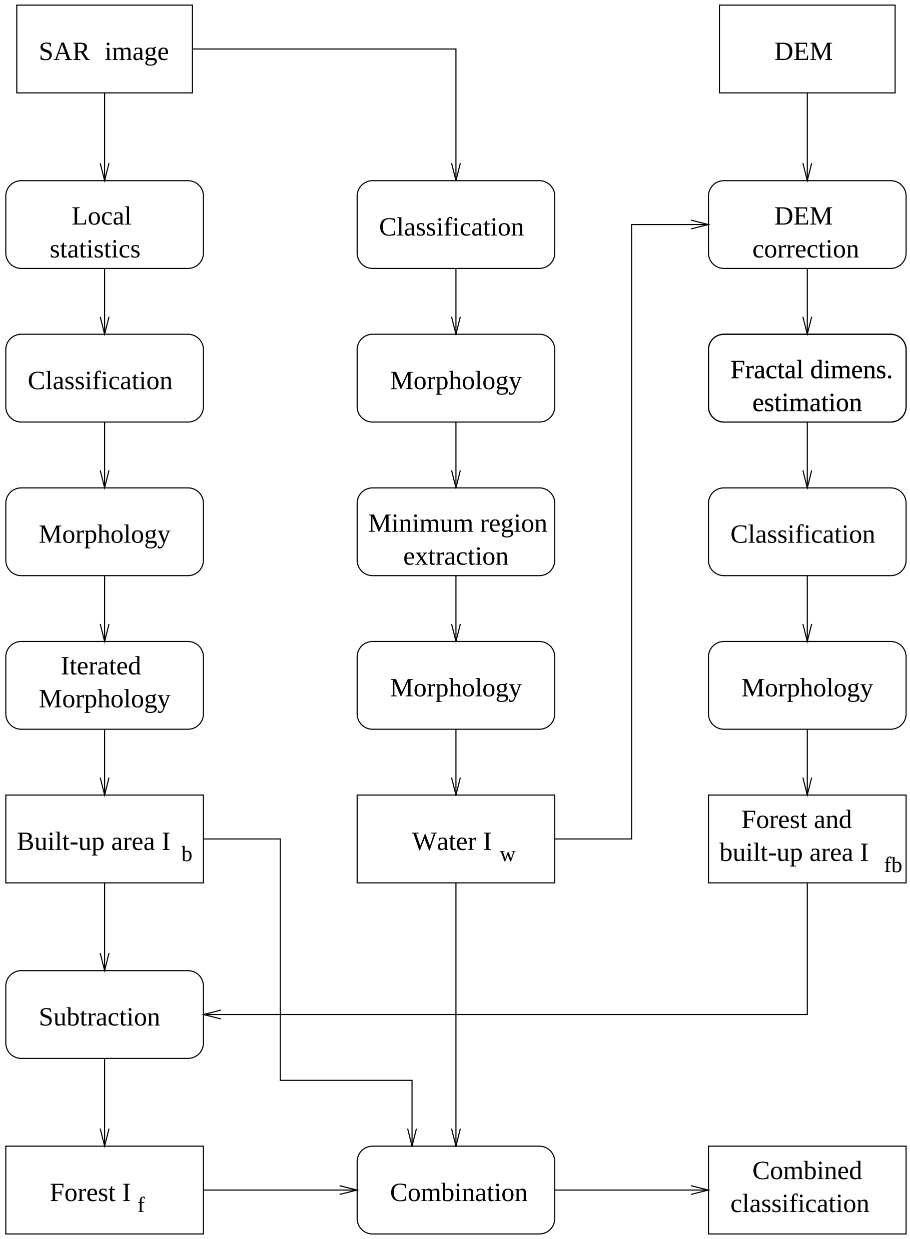

Figure 3. Data flow diagram of the classification algorithm. The sources of information are the SAR intensity image and the DEM at the top, the classification products are the square boxes at the bottom.

5. ASSESSMENT OF RESULTS

The result is assessed using overall accuracy and Kappa[13] and Tau[14] coefficient derived from confusion matrices. The reference categories were obtained by visual interpretation from the SAR backscatter image with the help of a topographic map. First we consider the results for the classification into four classes, secondly we investigate all classes different from the open area class. This is motivated by the fact that we are primarily interested in detection of the built–up and forest class for the purpose of bare–soil DEM approximation. This is also the reason to accecpt a low map producers accuracy for this special class. Table 1 shows the confusion matrix of the decision tree classification. Table 2 gives values for the overall accuracy and Kappa and Tau. The second line of table 2 shows the relevant values for the task at hand.

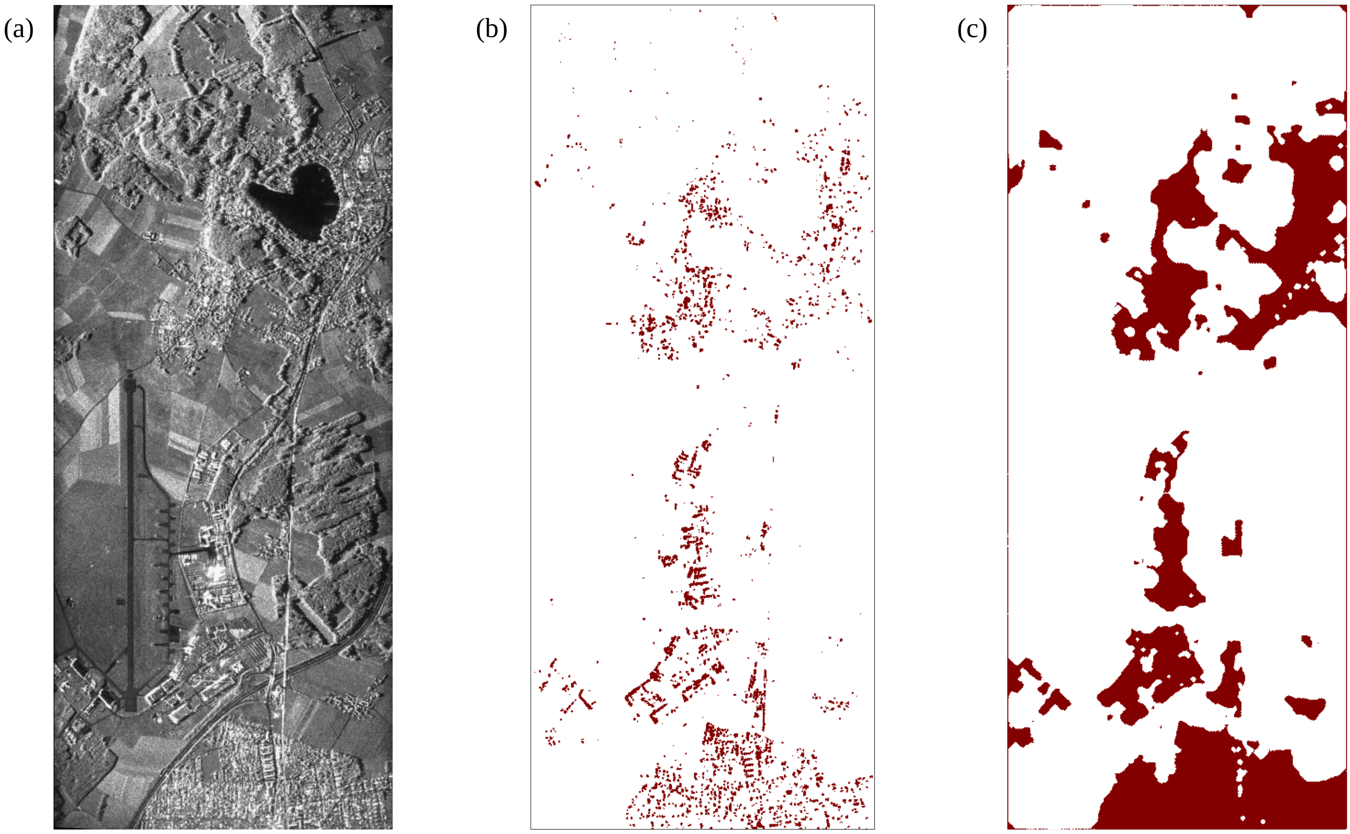

Figure 4. (a) AES–1 image of Oberpfaffenhofen testsite, (b) Classification of built–up area using local variance of backscatter image, (c) Improved classification by iterated mathematical morphology

Table 1. Confusion matrix of the decision tree classification into four classes.

Classifed category	Reference category Class 1 Water	Class 2 Built–up	Class 3 Forest	Class 4 Open area	Producers accuracy [%]
Water	137015	1935	743	0	96.06
Built–up	3420	1984051	78770	547091	89.63
Forest	0	154733	1643591	802709	89.73
Open area	2203	72945	108675	4554663	77.14

For completeness, the definition of Kappa is given as

$$\kappa = \frac{N \sum_{i=1}^{r} x_{ii} - \sum_{i=1}^{r} (x_{i+} x_{+i})}{N^2 - \sum_{i=1}^{r} (x_{i+} x_{+i})}, \tag{10}$$

where N is the total number of observations, r is the number of rows in the confusion matrix, $x_i i$ is the number of oberservations in the main diagonal in row i, x_{i+} is the row sum for row i and x_{+i} the column sum for column i. The Tau coefficient is defined similar to Kappa, in our case we restricted ourself to measure τ_e, e.g. we assume equal a priori probabilities for class membership (see Ma and Redmond[14] for a complete discussion on Tau):

$$\tau_e = \frac{\frac{1}{N} \sum_{i=1}^{r} x_{ii} - \frac{1}{r}}{1 - \frac{1}{r}}. \tag{11}$$

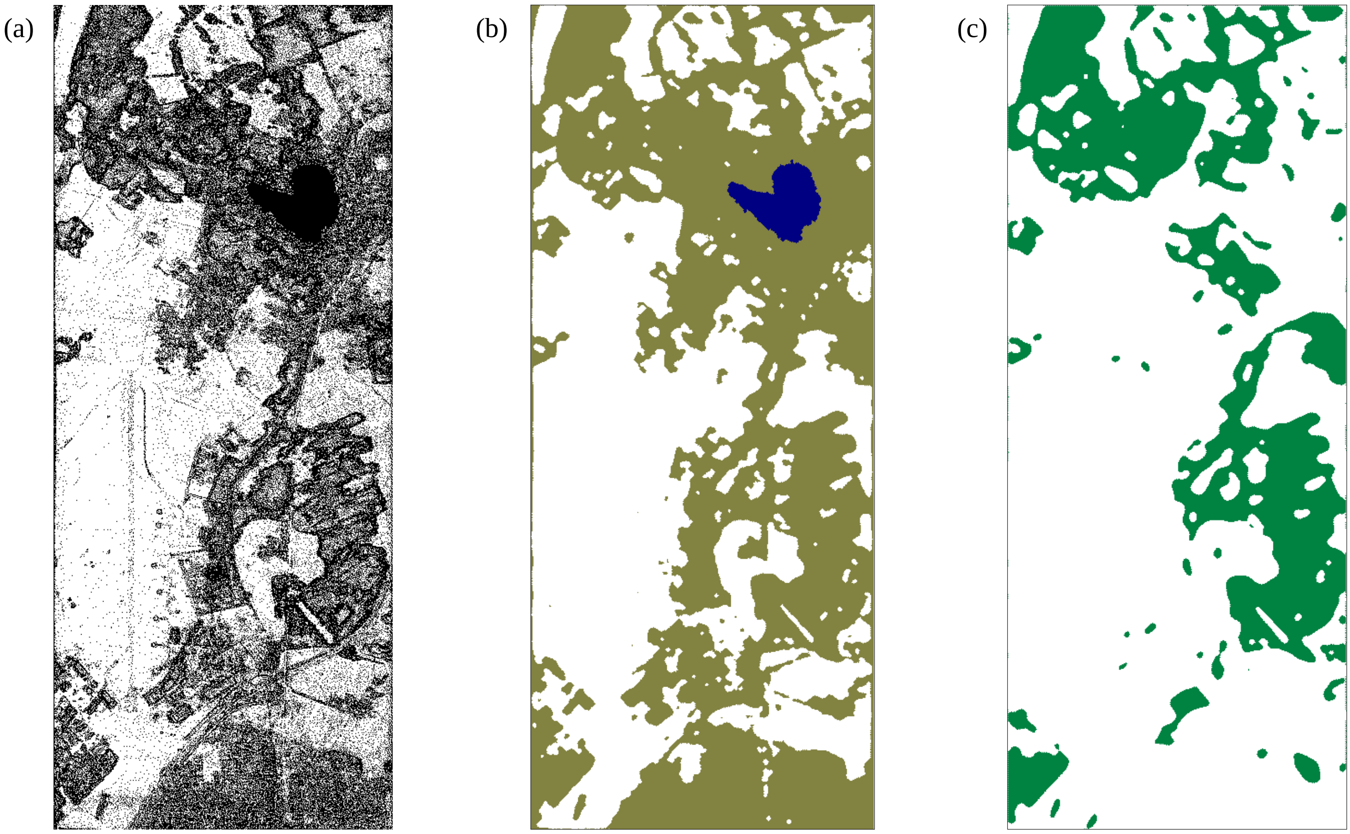

Figure 5. (a) Estimated fractal dimension of the DEM, (b) Classified and morphologically closed fractal dimension, (c) Classification of forest obtained by subtracting classified build–up area from the combined forest and built–up area classification.

Tau can be seen as a measure of improvement over random assignment, additionally τ_e is independent from class size.

Table 2. Assessement of the classification into four classes and three relevant classes.

Number of classes	Overall accuracy	Kappa κ	Tau τ_e
4	0.832837	0.719091	0.777116
3	0.924789	0.859754	0.887183

6. CONCLUSIONS

We have presented the ability to automatically derive cartographic information from airborne AeS–1 SAR data. The decision tree leads to a simple algorithm well suited to the task at hand. The high resolution of the AeS–1 data results in a highly accurate classification, which reduces manual post-processing in cartographic product generation.

Future work will use the classification of built–up and forest areas to automatically approximate a Digital Terrain Model from the interferometrically produced DEM. Further work will incorporate P–band data which can be used to extract the DEM in areas covered by forest, nevertheless the considerations presented in this paper provide additional information and remain important for built–up areas.

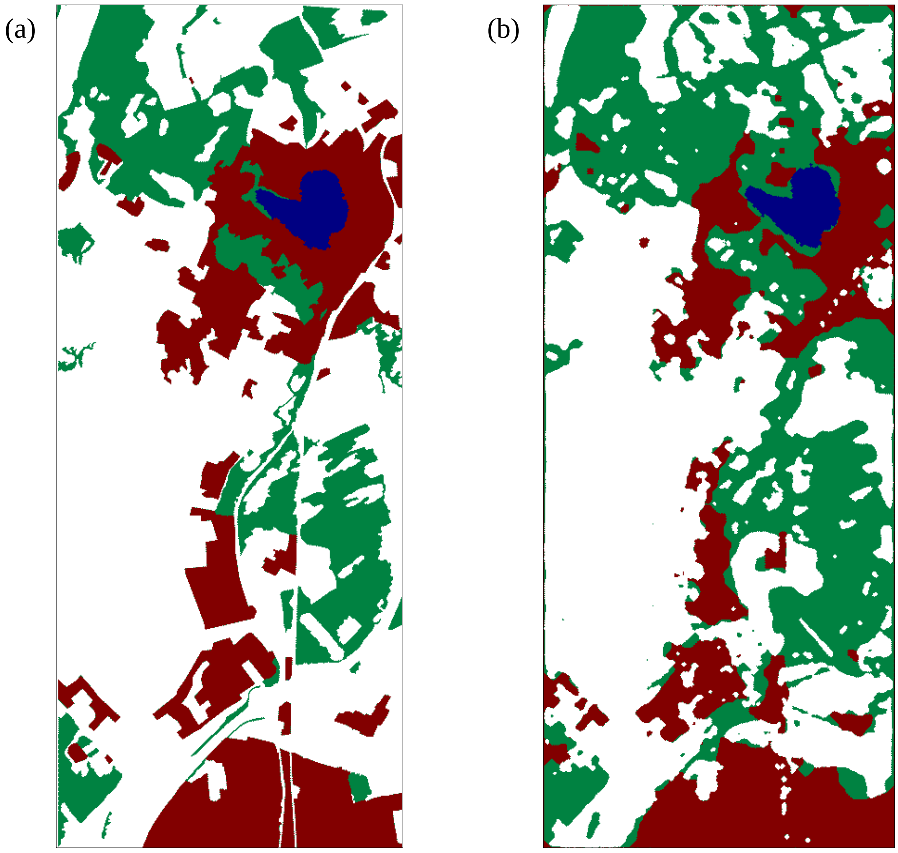

Figure 6. (a) Visual interpretation of radar backscatter, (b) Automatic classification from backscatter and coherence data by a decision tree.

ACKNOWLEDGEMENTS

This work is a joint work between Aero–Sensing GmbH and the Department of Cartography, Polytechnic University of Munich, represented by Theodor Wintges.

REFERENCES

1. M. Schwäbisch, *Die SAR–Interferometrie zur Erzeugung digitaler Geländemodelle*. PhD thesis, Fakultät für Bauingenieur- und Vermessungswesen, Universität Stuttgart, 1995.
2. U. Wegmüller and C. Werner, "Retrieval of Vegetation Parameters with SAR Interferometry," *IEEE Transactions on Geoscience and Remote Sensing* **35**, pp. 18–24, Jan. 1997.
3. J. Moreira, "Design of an Airborne Interferometric SAR for High Precision DEM Generation," in *XVIII ISPRS Congress, Vol. XXI, Part B2, Commission II*, pp. 256–260, (Vienna, Austria), 1996.
4. A. Pentland, "Fractal–Based Description of Natural Scenes," *IEEE Transactions on Pattern Analysis and Machine Intelligence* **6**, pp. 661–674, Nov. 1984.
5. M. Migliaccio and D. Riccio, "Fractal Brownian Model for SAR Image Analysis: Edge Detection and Classification Issues," in *Proceedings of the International Geoscience and Remote Sensing Symposium*, pp. 1605–1607, (Tokyo, Japan), Aug. 1993.
6. B. B. Mandelbrot, *The Fractal Geometry of Nature*, W.H. Fremann, 1982. ISBN 0–7167–1186–9.
7. R. M. Haralick, S. R. Sternberg, and X. Zhuang, "Image Analysis Using Mathematical Morphology," *IEEE Transactions on Pattern Analysis and Machine Intelligence* **9**, pp. 532–550, July 1987.
8. R. M. Haralick, K. Shanmugam, and I. Dinstein, "Textural Features for Image Classification," *IEEE Transactions on Systems, Man and Cybernetics* **3**, pp. 610–621, Nov. 1973.

9. P. Ferrazzoli, S. Paloscia, P. Pampaloni, G. Schiavon, S. Sigismondi, and D. Solimini, “The Potential of Multifrequency Polarimetric SAR in Assessing Agricultural and Arboreous Biomass,” *IEEE Transactions on Geoscience and Remote Sensing* **35**, pp. 5–17, Jan. 1997.
10. S. R. Sternberg, “Grayscale Morphology,” *Computer Vision, Graphics and Image Processing* **35**, pp. 333–355, 1986.
11. A. C. Frery and A. L. B. Candeias, “On the Improvement of 1-look SAR Image Segmentations with Mathematical Morphology,” in *Proceedings of SPIE*, vol. 2315, pp. 245–255, 1994. ISBN 0–8194–1645–2.
12. S.-C. Pei and C.-L. Lai, “An Efficient Class of Alternating Sequential Filters in Morphology,” *Computer Vision, Graphics and Image Processing: Graphical Models and Image Processing* **59**, pp. 109–116, Mar. 1997.
13. R. G. Congalton, “A Review of Assessing the Accuracy of Classifications of Remotely Sensed Data,” *Remote Sensing of Environment* **37**, pp. 35–46, 1991.
14. Z. Ma and R. L. Redmond, “Tau Coefficients for Accuracy Assessment of Classification of Remote Sensing Data,” *Photogrammetric Engineering and Remote Sensing* **61**, pp. 435–439, Apr. 1995.